

Generalized predictive control strategy applied to a single-phase T-type voltage source inverter in stand-alone operation mode

Diego Naunay

Department of Electrical and
Electronics Engineering
Universidad de las Fuerzas Armadas
ESPE

Sangolquí, Ecuador
dfnaunay@espe.edu.ec

Wilmar Martinez

Department of Electrical Eengineering,
ESAT
KU Leuven

Diepenbeek, Belgium
wilmar.martinez@kuleuven.be

Paúl Ayala

Department of Electrical and
Electronics Engineering
Universidad de las Fuerzas Armadas
ESPE

Sangolquí, Ecuador
jpayala@espe.edu.ec

Jaqueline Llanos

Department of Electrical and
Electronics Engineering
Universidad de las Fuerzas Armadas
ESPE

Sangolquí, Ecuador
jdllanos1@espe.edu.ec

Josue Andino

Department of Electrical and
Electronics Engineering
Universidad de las Fuerzas Armadas
ESPE

Sangolquí, Ecuador
jaandino@espe.edu.ec

Diego Arcos-Aviles

Department of Electrical and
Electronics Engineering
Universidad de las Fuerzas Armadas
ESPE

Sangolquí, Ecuador
dgarcos@espe.edu.ec

Abstract—This paper details a voltage control strategy based on Generalized Predictive Control (GPC) applied to a single-phase T-type neutral point clamped voltage source inverter in stand-alone operation mode. A performance comparison between the GPC and a Proportional-Integral (PI) controller is presented to highlight the improved performance of GPC under different load scenarios. The main results show that the GPC can achieve longer prediction horizons than other controllers based on model predictive control. Furthermore, in contrast to the PI controller, the GPC responds to load changes as disturbances. Finally, GPC can operate efficiently without an online optimization method nor recursive system identification method.

Index Terms—generalized predictive control, control strategy, voltage source inverter, multilevel inverter, single-phase T-type inverter

I. INTRODUCTION

Economic and industrial development has led to a progressive increase in the worldwide electricity demand. However, the excessive use of fossil fuels has generated environmental problems, categorizing this energy source as costly, unsafe, inadequate, and generating high levels of environmental pollution [1]. Renewable Energy Sources (RES) have emerged as a sustainable alternative to solve this problem [2]. Thus, by 2030, the International Energy Agency (IEA) projects that RES will cover 80% of the worldwide electricity growth [3].

Photovoltaic (PV) energy is a kind of RES that has become attractive due to its low pollution level [4]. However, this

source generates DC power, and most domestic and industrial loads require an AC source. Therefore, it is necessary to use a DC-AC converter, also known as an inverter [5]. Depending on the power source of an inverter, they can be classified between: Voltage Source Inverters (VSIs) and Current Source Inverters (CSIs) [6]. VSIs can operate connected to the grid, or they can work in stand-alone mode. In grid-connected mode, the VSI injects current to the grid so that the primary variable to control is the system current. Conversely, in stand-alone mode, the VSI generates a voltage for the isolated grid. Therefore, the system voltage becomes the primary control variable [7].

Several algorithms are used to control VSIs, such as voltage oriented control, sliding mode control, fuzzy control, among others [8]. However, Model Predictive Control (MPC) has been the most developed during the last decade [9]. Two types of MPC controllers applied to inverters can be distinguished: Finite Control Set (FCS-MPC) and Continuous Control Set (CCS-MPC) [10]. On the one hand, the FCS-MPC is more developed due to its easy and intuitive implementation. However, it presents two main drawbacks when implemented. The first is the variable switching frequency, which increases the Total Harmonic Distortion (THD) and switching losses. The other is an exponential growth of the computational burden in the cost function optimization as the prediction horizon increases [11]. Moreover, the CCS-MPC-based controllers, such as Generalized Predictive Control (GPC), have gained importance in recent years since they allow switching at a fixed frequency and longer prediction horizons, which provides for lower THD, switching losses, and computational cost [12].

Several studies on GPC applied to inverters are focused on grid-connected systems. The authors in [13] propose an adaptive GPC for a single-phase grid-connected inverter to ensure smooth control of active and reactive power. This work uses a plant identification system and highlights the improved performance of GPC when compared with a linear controller. Moreover, the study in [14] presents a GPC for a Three-Level (3L) VSI in full-bridge topology connected to the grid. This work's main result consists of eliminating the third, fifth, and seventh order harmonics while reaching a correct tracking to the sinusoidal reference. Furthermore, a GPC of a three-phase two-level grid-connected voltage system is described in [15]. This work shows a reduction of the THD compared to a resonant proportional controller. However, non-linear loads are not considered in this study. Finally, the authors in [16] present a further study of the work developed in [15], achieving a higher stability margin by changing the output filter for a third-order filter.

Based on the previous works and up to the authors' knowledge, a single-phase multilevel VSI in a stand-alone operation mode based on the GPC has not been analyzed so far. Only two-level and grid-connected inverters have been widely studied. The importance of analyzing stand-alone systems consists in providing energy solutions to improve electricity access in isolated areas [17]. In addition, research on multilevel VSIs has advantages over two-level ones since they produce less THD and allow the switching devices to operate with less voltage [18]. Therefore, this study proposes a novel control strategy based on GPC applied to a single-phase 3L T-type Neutral Point Clamped (NPC) VSI. The proposed strategy uses the Park transformation to generate the direct, quadrature and zero voltage components in a rotating reference frame. This transformation is achieved through a voltage Orthogonal Signal Generator (OSG), which generates the voltage components in a stationary orthogonal reference frame required for the Park transformation. Consequently, the GPC controls the VSI peak voltage instead of its RMS voltage. In addition, this study uses an offline optimization procedure for the cost function, considering the change of loads as disturbances. Finally, a comparison with the results achieved by a PI controller for different load scenarios is presented.

The main contributions of this work are detailed as follows. (i) This study proposes a methodology of a GPC applied to a single-phase multilevel VSI in stand-alone operation mode. (ii) The implementation of an MPC with a large prediction horizon without high computational cost.

The paper is organized as follows. Section II presents the mathematical model and control strategy of the system. Section III details the performance results achieved by the PI and GPC controllers against different load scenarios. Section IV presents a discussion regarding the obtained results. Finally, Section V summarizes the main conclusions of this work.

II. SYSTEM MODELING

Fig. 1 shows the proposed single-phase 3L T-type NPC VSI control loop. This system comprises two series DC voltage

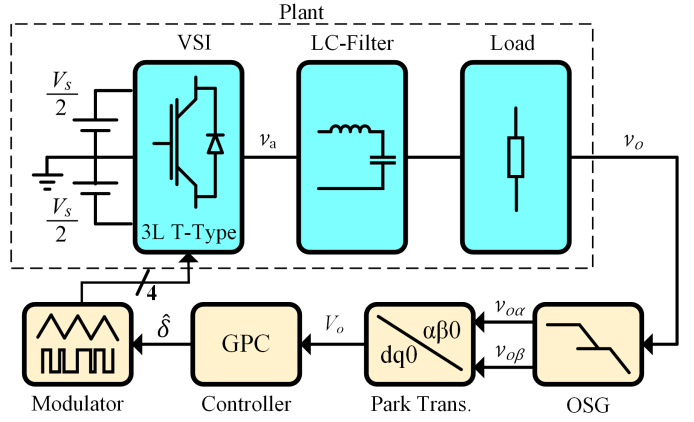


Fig. 1. Proposed generalized predictive control loop for a 3L T-type NPC VSI

sources, the power switches connected in T-type configuration, an *LC* (inductor-capacitor) filter, an OSG, a Park transformation block, the GPC, and a constant frequency modulator. From Fig. 1, the variable V_s represents the total DC-link input voltage, v_a denotes the common voltage node of the *LC* filter, v_o is the AC-link output voltage, $v_{o\alpha}$ and $v_{o\beta}$ represent the two voltage components in a stationary orthogonal reference frame, V_o denotes the peak voltage of v_o , and δ represents the duty cycle. Each of these components is discussed in detail below.

A. Single-phase 3L T-type NPC voltage source inverter

Multilevel VSIs achieve better power quality and fewer harmonics in the AC-link output voltage over two-level VSIs [18]. Several multilevel topologies can be found, such as cascade H-bridge, flying capacitor, NPC, among others [19]. However, the NPC has a more straightforward structure and lower switching losses than the other topologies [4], [20].

An NPC VSI is a three-level AC-DC converter with a high, a low, and a neutral level. The last one is generated by the common point of both DC sources. Several configurations of this topology can be distinguished, such as active NPC, stacked NPC, active and stacked NPC, and T-type NPC. However, the T-Type configuration stands out from the others due to its high efficiency, lower switching losses, and the optimization of the number of power devices it uses [20]. Fig. 2 shows a single-phase 3L T-type NPC VSI configuration with an output *LC* filter where the series resistor R_L represents the losses in L , resistor R denotes the load connected to the DC-AC converter output, i_L is the current flowing through L , and i_o represents the current flowing through the load.

This configuration consists of four switching devices, where power switches S_1 and S_3 have complementary control signals, as do switches S_2 and S_4 . The possible combinations of the ON and OFF states of the power switches, represented by the logical values 1 and 0 respectively, generate the three voltage levels at point a (v_a). Similarly, these states are related to the control switching actions (u), as detailed in Table I.

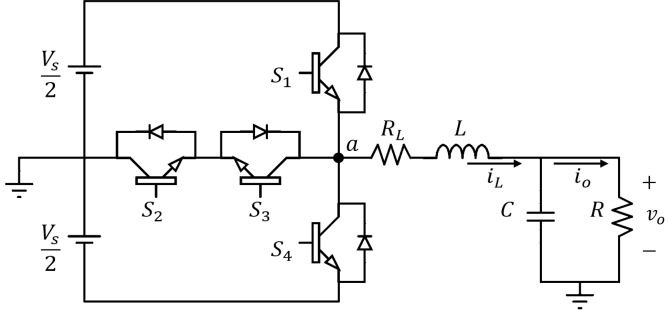


Fig. 2. Single-phase T-type NPC VSI configuration

TABLE I
RELATIONSHIP AMONG OUTPUT VOLTAGE AND SWITCHING STATES

S_1	S_2	S_3	S_4	Voltage v_a	u
1	1	0	0	$V_s/2$	1
0	1	1	0	0	0
0	0	1	1	$-V_s/2$	-1

The mathematical model of the T-type configuration is represented by the state-space model, as follows:

$$\begin{bmatrix} \dot{i}_L(t) \\ \dot{v}_C(t) \end{bmatrix} = \begin{bmatrix} -R_L & -\frac{1}{L} \\ \frac{1}{C} & -\frac{1}{RC} \end{bmatrix} \cdot \begin{bmatrix} i_L(t) \\ v_C(t) \end{bmatrix} + \begin{bmatrix} \frac{1}{L} \\ 0 \end{bmatrix} \cdot u_v(t) \quad (1)$$

$$v_o(t) = [0 \ 1] \cdot \begin{bmatrix} i_L(t) \\ v_C(t) \end{bmatrix}$$

where t is the time's variable, $u_v \in [-V_s/2, 0, V_s/2]$, and v_C is the capacitor voltage. Thus, the plant's transfer function (G_p), representing the relationship between v_o and u_v , is detailed in (2), as follows:

$$G_p(s) = \frac{\frac{1}{LC}}{s^2 + s \left(\frac{R_L}{L} + \frac{1}{RC} \right) + \frac{R + R_L}{RLC}} \quad (2)$$

B. LC-Filter design

The filter design is based on the inductance voltage, inductance ripple current, and cut-off filter frequency. Therefore, it attenuates the low harmonic frequency components. In this regard, the impedance should be minimized while maximizing the capacitance. The maximum voltage on the inductor (V_L) corresponds to the difference between the inverter's maximum input and output voltages, as follows [21]:

$$V_L = V_a - V_o \quad (3)$$

where V_a is the peak voltage of v_a . Note that the ratio between V_a and V_o corresponds to the duty cycle. As a result, the inductor voltage can be represented as a function of the input voltage, according to:

$$V_L = \frac{V_s}{2} \left(1 - \hat{\delta} \right) \quad (4)$$

Furthermore, the inductor voltage depends on the switching frequency of the power devices (f_s), the DC-link voltage, and the maximum inductor ripple current ($\Delta \hat{I}_L$), as detailed in (5) [21]. Hence, using (4) and (5), the inductance value is obtained as detailed in (6):

$$V_L = L \frac{\Delta \hat{I}_L}{\hat{\delta}} f_s \quad (5)$$

$$L = V_s \frac{\hat{\delta}(1 - \hat{\delta})}{2 \Delta \hat{I}_L f_s} \quad (6)$$

Similarly, the capacitance value is obtained through the ratio between the low-pass filter cut-off frequency and the switching frequency. According to [22], the cut-off frequency of the filter should be at least fifteen times smaller than f_s . Thus, C is computed as follows:

$$C \geq \frac{15^2}{(2 \pi f_s)^2 L} \quad (7)$$

C. Orthogonal signal generator and Park transformation

Most controllers applied to three-phase VSI use vector transformations to simplify the analysis of power circuits. The Clarke and Park transformations are the most commonly used. On the one hand, the Clarke transformation changes a three-phase system, with abc coordinates, to a stationary orthogonal reference frame, with $\alpha\beta$ coordinates. On the other hand, the Park transformation changes a system, with $\alpha\beta$ coordinates, to a rotating orthogonal reference frame, with dq coordinates. These transformations applied to a three-phase voltage system obtain a constant voltage signal equivalent to the peak of AC-link voltage, which simplifies the control input [23].

However, these transformations cannot be applied to a single-phase system since only a single voltage signal is present. In this case, an OSG is used to generate a system in a stationary orthogonal reference frame. Several types of OSG are available, such as OSG based on transport delay, inverse Park transform, derivative, low-pass filter, among others. However, the OSG based on second-order low-pass filter has been selected due to its high performance and lower computational cost when it is implemented [24]. Therefore, the transfer function of this OSG applied to v_o can be expressed according to:

$$\frac{\tilde{V}_{o\beta}(s)}{\tilde{V}_o(s)} = \frac{2 \omega_n^2}{s^2 + 2 \xi \omega_n + \omega_n^2} \quad (8)$$

where $\tilde{V}_{o\beta}$ and \tilde{V}_o are equivalent to $v_{o\beta}$ and v_o in s domain, respectively, ω_n represents the undamped natural frequency, and ξ is the damping ratio. Considering $\xi = 1$ and ω_n equivalent to the natural frequency of v_o signal, the filter input expressed in (8) will correspond to $v_{o\alpha}$, whereas the filter output will correspond to the stationary orthogonal component $v_{o\beta}$. Both components, through the Park transformation, generate the direct voltage signal (v_d), equivalent to the peak voltage V_o , and the quadrature voltage signal (v_q).

D. Generalized predictive control

The GPC is a type CCS-MPC based on the Controlled Auto-Regressive Integrated Moving Average (CARIMA) model. In this type of MPC, the control actions are a set of continuous-time signals sent to a modulator. Thus, most single-input single-output plants can be expressed as follows [12]:

$$A(z^{-1})y(t) = B(z^{-1})z^{-d}u_d(t-1) + C_d(z^{-1})\frac{e(t)}{1-z^{-1}} \quad (9)$$

where d is the number of discrete delays, $A(z^{-1})$ and $B(z^{-1})$ are the polynomials of the denominator and numerator, respectively, which represent the plant's transfer function as a function of the backward shift operator (z^{-1}), $u_d(t)$ is the control action equivalent to $\hat{\delta}$, $y(t)$ is the plant's output, $e(t)$ is a zero-mean white noise, and $C_d(z^{-1})$ is the measurable disturbance, which is set to 1 in the case of non-stationary disturbances.

The optimal prediction is obtained by solving the Diophantine equation [25]. In addition, the cost function (J) associated to the GPC is detailed in (10), as follows [12]:

$$\begin{aligned} J(N_p, N_c) = & \sum_{j=1}^{N_p} \delta(j) [\hat{y}(t+j | t) - w(t+j)]^2 + \dots \\ & \dots + \sum_{j=1}^{N_c} \lambda(j) [\Delta u_d(t+j-1)]^2 \end{aligned} \quad (10)$$

where $\hat{y}(t+j | t)$ is the optimal system output prediction j steps ahead on the data up to the time t , N_p and N_c are the prediction and control horizons, respectively, δ and λ are the weights of predictions and control components, respectively, Δu_d is the increment of u_d , and w is the reference trajectory, which represents the set-point. Note that J aims to minimize the control effort to make the future output follows the reference signal on the N_p horizon [25]. Thus, in [12], Δu_d for a time t is obtained as:

$$\Delta u_d(t) = \mathbf{K}(\mathbf{w} - \mathbf{f}) \quad (11)$$

where \mathbf{K} is a constant vector representing the control action applied to the error between the reference vector (\mathbf{w}) and the free response vector (\mathbf{f}). Both \mathbf{K} and \mathbf{f} values can be calculated from the CARIMA model and the Diophantine equation, as described in [25].

E. Pulse width modulator

The controller output corresponds to the duty cycle of the switching elements. This value is constrained between 0 and 1 through a saturation block. For this purpose, a carried-based unipolar modulator transforms the control action into a Pulse-Width Modulated (PWM) signals, as shown in Fig. 3 [26], [27].

As it can be seen in Fig. 3, CW_1 and CW_2 are the carrier waves, and v_m is the modulation wave. Signal v_m is a sine wave at the AC link nominal frequency (f_n). The crossings of CW_1 and CW_2 with v_m generate the PWM signals for each switch. The ratio between v_m amplitude (V_m) and the double

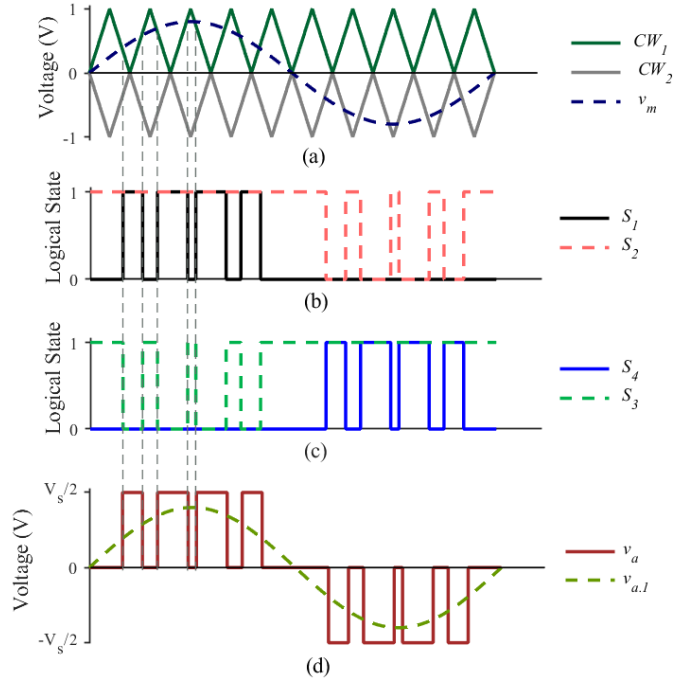


Fig. 3. Carried-based PWM for T-type NPC VSI. (a) Carried-based unipolar modulator. (b) Activation signals of switches S_1 and S_2 . (c) Activation signals of switches S_3 and S_4 . (d) 3L voltage at LC filter common node.

of CW_1 or CW_2 amplitude is equivalent to $\hat{\delta}$. In the case where the sum of CW_1 and CW_2 amplitudes is one, the values V_m and $\hat{\delta}$ are equal. Thus, v_m is obtained by multiplying $\hat{\delta}$ with a unitary amplitude sine wave.

III. SIMULATION AND RESULTS

The proposed control loop has been implemented in Matlab®-Simulink. This work assumes a nominal output current of $10 A_{RMS}$, a switching frequency of $20 kHz$, and a maximum inductor ripple current of 16.5% [21]. These values are used in (3) to (7) to compute the filter parameters. Table II summarizes the 3L T-type VSI simulation parameters.

The transfer function of the single-phase 3L T-type NPC VSI, detailed in (2), is discretized with the ZOH method at $50 \mu s$, as follows:

$$G_p(z) = \frac{0.02933z^{-1} + 0.02905z^{-2}}{1 - 1.9129z^{-1} + 0.97143z^{-2}} \quad (12)$$

TABLE II
ELEMENT VALUES OF THE SINGLE-PHASE 3L T-TYPE NPC VSI

Parameter	Description	Value	Unit
V_s	DC-link voltage	400	V
v_o	Nominal AC-link voltage	110	V_{RMS}
f_n	Nominal frequency	60	Hz
f_s	Switching frequency	20	kHz
L	Filter inductance	750	μH
R_L	Inductance resistance	100	$m\Omega$
C	Filter capacitance	56	μF
R	Output load	40	Ω

Based on the transfer function in (12), it is possible to find the values N_p , N_c , δ , and λ of the GPC. The correct selection of these parameters allows obtaining a system response without overshoot, a settling time less than 20 ms, and a THD less than 5%. Therefore, a system with no delay ($d = 0$), $N_p = N_c = N$ and $\delta = 1$ is considered for simplicity. On the one hand, the best results are obtained with $N \geq 9$ since the harmonic content increases with shorter prediction and control horizons. Likewise, concerning load disturbances, the controller decreases its response time with longer horizons.

On the other hand, various values of λ are tested. When this value is minimal, the system presents a faster response. However, the controller causes an oscillatory response in the system for a prolonged time. In contrast, as the λ value increases, the overshoot decreases and the system settling time increases. After several tests, the values of λ and N that fulfills the design requirements are 390 and 9, respectively.

A PI controller with a parallel architecture is implemented to contrast the results achieved by the GPC. The controller gains ($K_i = 1.5$ and $K_p = 0.0025$) are tuned according to the same performance parameters detailed for the GPC. In this regard, three scenarios are considered for testing the performance of both controllers. The first one uses different resistive loads. The second one includes some RL loads. Finally, the last one assumes a non-linear load based on a wave rectifier with a parallel RC load. In addition, two measurement criteria are chosen to analyze the controllers' performance: the THD in steady-state and the settling time (t_s). Each test is performed for 0.3 s in the different scenarios, which results are detailed in Table III, Table IV, and Table V.

Moreover, Fig. 4, Fig. 5, and Fig. 6 show the responses of both controllers under different load perturbations. For each case, the initial load is 50Ω and the perturbation is placed in parallel of the initial load at $t = 104.17$ ms. Fig. 4 presents

TABLE V
SCENARIO 3: PERFORMANCE AT DIFFERENT NON-LINEAR LOADS BASED ON WAVE RECTIFIER WITH RC LOAD

Load		GPC Controller		PI Controller	
		THD (%)	t_s (ms)	THD (%)	t_s (ms)
Case 1	$R = 500 (\Omega)$ $C = 330 (\mu F)$	3.58	12.60	5.26	18.60
Case 2	$R = 200 (\Omega)$ $C = 330 (\mu F)$	6.40	12.30	7.08	19.20
Case 3	$R = 100 (\Omega)$ $C = 330 (\mu F)$	9.43	12.05	8.51	18.10

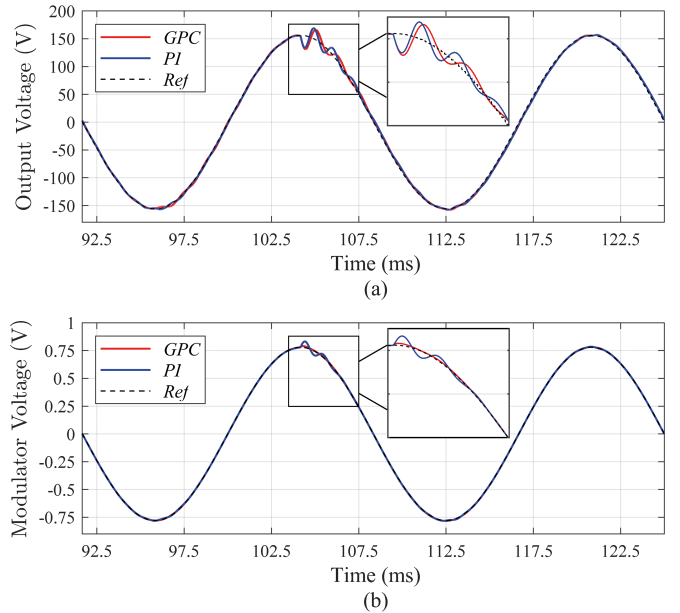


Fig. 4. Response of the GPC and PI controllers under a resistive load disturbance at $t = 104.17$ ms. (a) Output AC-link voltage waveform. (b) Control action applied at the system modulator.

TABLE III
SCENARIO 1: PERFORMANCE AT DIFFERENT RESISTIVE LOADS

Load $R (\Omega)$	GPC Controller		PI Controller	
	THD (%)	t_s (ms)	THD (%)	t_s (ms)
1000	2.58	12.60	154.14	-
200	2.12	12.60	73.56	-
100	1.56	12.60	3.61	20.00
50	1.41	12.40	1.25	19.40
20	0.66	12.40	0.74	19.50
10	0.66	12.45	0.68	19.00

TABLE IV
SCENARIO 2: PERFORMANCE AT DIFFERENT RL LOADS

Load		GPC Controller		PI Controller	
		THD (%)	t_s (ms)	THD (%)	t_s (ms)
Case 1	$R = 50 (\Omega)$ $L = 10 (mH)$	1.51	12.50	3.65	19.00
Case 2	$R = 50 (\Omega)$ $L = 20 (mH)$	1.80	12.50	94.02	-
Case 3	$R = 50 (\Omega)$ $L = 50 (mH)$	1.91	12.60	161.90	-

the response under a resistive load disturbance of 20Ω . Fig. 5 depicts the system's response under a RL load disturbance ($R = 50 \Omega$ and $L = 10 mH$). Finally, Fig. 6 shows the response under a non-linear load disturbance based on a wave rectifier with parallel RC load ($R = 200 \Omega$ and $C = 330 \mu F$).

IV. DISCUSSION

The simulation of the control strategy shown in Fig. 1 evidences that OSG based on second-order low-pass filter allows the Park transformation to obtain a constant value of the controller reference and a system output equivalent to V_o . As a result, an improved controller performance is achieved due to its faster response regarding the RMS-based controller.

Moreover, the controller's optimization is performed offline, making it possible to consider load changes as disturbances. In the first scenario detailed in Table III, the performance of controllers for the different resistive loads is tested. Although the controller does not have a recursive plant identification, the THD values are kept below 2.6%, and the settling time

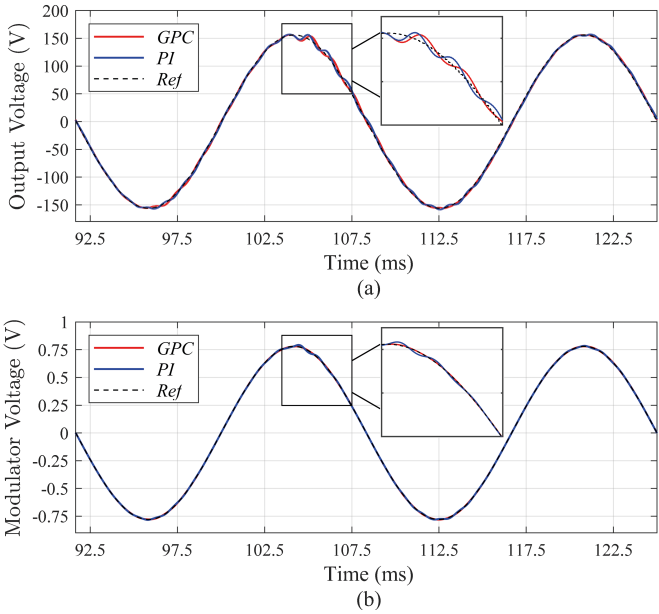


Fig. 5. Response of the GPC and PI controllers under a RL load disturbance at $t = 104.17\text{ ms}$. (a) Output AC-link voltage waveform. (b) Control action applied at the system modulator.

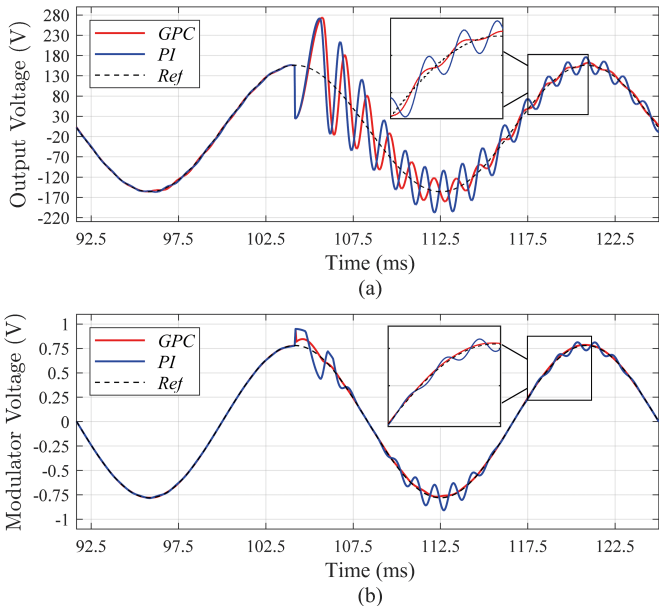


Fig. 6. Response of the GPC and PI controllers to under a non-linear load based on a wave rectifier with parallel RC load at $t = 104.17\text{ ms}$. (a) Output AC-link voltage waveform. (b) Control action applied at the system modulator.

is approximately 12.6 ms for each case. Conversely, the PI controller cannot control the system when the loads are low, resulting in high THD values and system instability. Similar behavior is obtained in the second scenario, as shown in Table IV. In this scenario, the GPC manages the RL loads despite not being designed for this purpose. The THD does not exceed 2%, in contrast to the PI controller, which fails to control loads

with a significant inductance value.

In the third scenario detailed in Table V, the GPC maintains a THD of less than 8% for low values of non-linear loads. This THD is the minimum value required for systems below 1KV. However, for high non-linear loads, the THD value exceeds the maximum recommended in [28]. Conversely, the PI controller presents better performance for high non-linear loads. Nevertheless, it still exceeds the maximum THD recommended since both controllers are designed for resistive loads.

In addition, as shown in Fig. 4 and Fig. 5, the GPC achieves a faster response and fewer harmonics in the transient state than the PI controller. Conversely, in Fig. 6, the transient stage presents a high harmonic content due to the non-linear current driving the load. Non-linear loads produce a high harmonic response due to their non-linear nature, causing a high injection of harmonic content into the network.

Finally, the GPC can adapt to various linear loads and some non-linear loads without changing the plant online, making the controller robust to high load variations.

V. CONCLUSION

This paper has presented a novel control strategy based on Generalized Predictive Control applied to a single-phase 3L T-type NPC VSI. The proposed GPC has been compared with a PI controller to contrast the performance results under different load scenarios. On tests performed with different R and RL loads, the GPC has achieved a settling time of less than 12.7 ms and a THD below 2.6% in steady-state. Thus, load changes could be considered as disturbances on the plant. In contrast, the PI controller becomes unstable under specific R and RL loads. However, in steady-state, an increase of THD has been observed in both controllers for non-linear loads due to the system's non-linear dynamics. In this regard, the simulation results have proved that the GPC can operate under different R and RL load scenarios without online optimization nor recursive identification of plant parameters. Consequently, the GPC could be considered a robust controller applied to single-phase 3L T-type NPC VSIs.

Future work will focus on: (i) the implementation of constraints in the GPC, such as on the overshoot or the control action, to improve the controller performance, (ii) the embedding and experimental validation of the control strategy with a microcontroller, and (iii) to propose a solution for non-linear loads based on GPCs.

ACKNOWLEDGMENT

This work is part of the project 2020-EXT-007 “MIRATESTE: Specific, innovative microgrids solutions (accounting for environmental, social, technological and economic aspects) for isolated rural areas of Ecuador” from Universidad de las Fuerzas Armadas ESPE and KU Leuven. This work has been developed with the support of VLIR-UOS and the Belgian Development Cooperation (DGD) under the project EC2020SIN322A101.

REFERENCES

- [1] M. E. Meral and D. Çelik, "A comprehensive survey on control strategies of distributed generation power systems under normal and abnormal conditions," *Annual Reviews in Control*, vol. 47, pp. 112–132, Jan. 2019.
- [2] M. A. Memon, S. Mekhilef, M. Mubin, and M. Aamir, "Selective harmonic elimination in inverters using bio-inspired intelligent algorithms for renewable energy conversion applications: A review," *Renewable and Sustainable Energy Reviews*, vol. 82, no. 3, pp. 2235–2253, Feb. 2018.
- [3] International Energy Agency, "World Energy Outlook 2020," International Energy Agency, Paris, Tech. Rep., 2020. [Online]. Available: <https://www.iea.org/reports/world-energy-outlook-2020>
- [4] N. Prabaharan and K. Palanisamy, "A comprehensive review on reduced switch multilevel inverter topologies, modulation techniques and applications," *Renewable and Sustainable Energy Reviews*, vol. 76, pp. 1248–1282, Sep. 2017.
- [5] A. A. Mohamed, H. Metwally, A. El-Sayed, and S. I. Selem, "Predictive neural network based adaptive controller for grid-connected PV systems supplying pulse-load," *Solar Energy*, vol. 193, pp. 139–147, Nov. 2019.
- [6] F. L. Luo and H. Ye, *Advanced DC/AC Inverters: Applications in Renewable Energy*, 1st ed. Boca Raton, FL: CRC Press, 2017.
- [7] A. Chatterjee and K. B. Mohanty, "Current control strategies for single phase grid integrated inverters for photovoltaic applications-a review," *Renewable and Sustainable Energy Reviews*, vol. 92, pp. 554–569, Sep. 2018.
- [8] S. Tahir, J. Wang, M. H. Baloch, and G. S. Kaloi, "Digital control techniques based on voltage source inverters in renewable energy applications: A review," *Electronics*, vol. 7, no. 2, p. 18, Feb. 2018.
- [9] W. R. Sultana, S. K. Sahoo, S. Sukchai, S. Yamuna, and D. Venkatesh, "A review on state of art development of model predictive control for renewable energy applications," *Renewable and Sustainable Energy Reviews*, vol. 76, pp. 391–406, Sep. 2017.
- [10] F. Sebaaly and H. Y. Kanaan, "New voltage vector generation method for a MPC algorithm with constant switching frequency operation," in *2017 IEEE 26th International Symposium on Industrial Electronics (ISIE)*, Jun. 2017, pp. 1692–1698.
- [11] J. H. Lee, J. S. Lee, H. C. Moon, and K. B. Lee, "An improved finite-set model predictive control based on discrete space vector modulation methods for grid-connected three-level voltage source inverter," *IEEE Journal of Emerging and Selected Topics in Power Electronics*, vol. 6, no. 4, pp. 1744–1760, Dec. 2018.
- [12] C. Bordons, F. Garcia-Torres, and M. A. Ridao, "Microgrids power quality enhancement," in *Model Predictive Control of Microgrids*, 1st ed. Switzerland: Springer International Publishing, 2020, ch. 9, pp. 227–261.
- [13] V. L. Srinivas, B. Singh, and S. Mishra, "Adaptive generalized predictive control scheme for single phase GPV system," in *2018 4th International Conference on Universal Village (UV)*, Oct. 2018, pp. 1–6.
- [14] D. M. Lima, V. F. Montagner, and L. A. Maccari, "Generalized predictive control with harmonic rejection applied to a grid-connected inverter with LCL filter," in *14th Brazilian Power Electronics Conference (COBEP)*, Nov. 2017, pp. 1–6.
- [15] M. G. Judewicz, S. A. Gonzalez, N. I. Echeverria, J. R. Fischer, and D. O. Carrica, "Generalized Predictive Current Control (GPCC) for Grid-Tie Three-Phase Inverters," *IEEE Transactions on Industrial Electronics*, vol. 63, no. 7, pp. 4475–4484, Jul. 2016.
- [16] M. G. Judewicz, S. A. Gonzalez, J. R. Fischer, J. F. Martinez, and D. O. Carrica, "Inverter-side current control of grid-connected voltage source inverters with LCL filter based on generalized predictive control," *IEEE Journal of Emerging and Selected Topics in Power Electronics*, vol. 6, no. 4, pp. 1732–1743, Dec. 2018.
- [17] M. Rodríguez, A. Salazar, D. Arcos-Aviles, J. Llanos, W. Martínez, and E. Motoasca, "A brief approach of microgrids implementation in Ecuador: A review," in *Recent Advances in Electrical Engineering, Electronics and Energy*, Mar. 2021, pp. 149–163.
- [18] Z. Boussada, O. Elbeji, and M. Benhamed, "Modeling of diode clamped inverter using SPWM technique," in *2017 International Conference on Green Energy Conversion Systems (GECS)*, Mar. 2017, pp. 1–5.
- [19] Y. Yang, H. Wen, M. Fan, M. Xie, R. Chen, and Y. Wang, "A constant switching frequency model predictive control without weighting factors for T-type single-phase three-level inverters," *IEEE Transactions on Industrial Electronics*, vol. 66, no. 7, pp. 5153–5164, Jul. 2019.
- [20] F. Sebaaly, H. Y. Kanaan, and N. Moubayed, "Three-level neutral-point-clamped inverters in transformerless PV systems - State of the art," in *2014 17th IEEE Mediterranean Electrotechnical Conference - MELECON*, Apr. 2014, pp. 1–7.
- [21] K. H. Ahmed, S. J. Finney, and B. W. Williams, "Passive filter design for three-phase inverter interfacing in distributed generation," in *2007 Compatibility in Power Electronics*, Jun. 2007, pp. 1–9.
- [22] S. Mondal, P. K. Gayen, and K. Gupta, "Study on impact of LC-filter parameters under variable loading conditions of three-phase voltage source inverter," in *2018 IEEE Electron Device Kolkata Conference, EDKCON*, Nov. 2018, pp. 132–136.
- [23] M. Ciobotaru, "Reliable grid condition detection and control of single-phase distributed power generation systems," Ph.D. dissertation, Aalborg University, Aalborg, 2009.
- [24] P. Lamo, A. Pigazo, and F. J. Azcondo, "Evaluation of quadrature signal generation methods with reduced computational resources for grid synchronization of single-phase power converters through phase-locked loops," *Electronics*, vol. 9, no. 12, p. 2026, Nov. 2020.
- [25] E. F. Camacho and C. Bordons, "Generalized predictive control," in *Model Predictive Control*, 2nd ed. London: Springer International Publishing, 2007, ch. IV, pp. 47–79.
- [26] P. Liu, S. Duan, C. Yao, and C. Chen, "A double modulation wave CBPWM strategy providing neutral-point voltage oscillation elimination and CMV reduction for three-level NPC inverters," *IEEE Transactions on Industrial Electronics*, vol. 65, no. 1, pp. 16–26, Jan. 2018.
- [27] B. L. Dokić and B. Blanuša, *Power Electronics: Converters and Regulators*, 3rd ed. Switzerland: Springer International Publishing, 2015.
- [28] IEEE Power and Energy Society, "IEEE Recommended Practice and Requirements for Harmonic Control in Electric Power Systems," New York, 2014. [Online]. Available: <https://standards.ieee.org/standard/519-2014.html>